Published in final edited form as:
Anal Bioanal Chem. 2010 January ; 396(1): 105–114. doi:10.1007/s00216-009-2971-x.

Molecular sputter depth profiling using carbon cluster beams

Andreas Wucher and
Fakultät für Physik, Universität Duisburg-Essen, 47048 Duisburg, Germany

Nicholas Winograd
Department of Chemistry, Pennsylvania State University, 104 Chemistry Bldg., University Park, PA 16802, USA

Andreas Wucher: andreas.wucher@uni-due.de

Abstract

Sputter depth profiling of organic films while maintaining the molecular integrity of the sample has long been deemed impossible because of the accumulation of ion bombardment-induced chemical damage. Only recently, it was found that this problem can be greatly reduced if cluster ion beams are used for sputter erosion. For organic samples, carbon cluster ions appear to be particularly well suited for such a task. Analysis of available data reveals that a projectile appears to be more effective as the number of carbon atoms in the cluster is increased, leaving fullerene ions as the most promising candidates to date. Using a commercially available, highly focused C_{60}^{q+} cluster ion beam, we demonstrate the versatility of the technique for depth profiling various organic films deposited on a silicon substrate and elucidate the dependence of the results on properties such as projectile ion impact energy and angle, and sample temperature. Moreover, examples are shown where the technique is applied to organic multilayer structures in order to investigate the depth resolution across film-film interfaces. These model experiments allow collection of valuable information on how cluster impact molecular depth profiling works and how to understand and optimize the depth resolution achieved using this technique.

Keywords

Molecular depth profiling; Cluster SIMS; Carbon clusters; Cluster ion beams

Introduction

The chemical characterization of molecular thin film structures still poses a difficult problem in modern surface analysis. Sputter depth profiling is one of the most versatile techniques to obtain in-depth chemical information about inorganic substrates with high surface sensitivity. It has long been deemed impossible to use this strategy for analysis of molecular films, because the ion beam employed to erode the surface inevitably compromises the molecular integrity of the sample. More specifically, molecules present at the surface are fragmented by the projectile ion impact, and the resulting chemical damage accumulates with increasing primary ion fluence. This effect leads to the establishment of a chemically altered surface layer which then persists during the entire erosion process. As a consequence, surface-sensitive analytical tools probing the chemistry of the momentary surface exposed by the erosion process deliver little more than elemental information with no chemical specificity. In particular, the molecular information obtained in mass spectrometric techniques such as secondary ion or neutral mass

Correspondence to: Andreas Wucher, andreas.wucher@uni-due.de.

spectrometry (SIMS or SNMS, respectively) is known to be rapidly compromised as a function of increasing primary ion fluence [1]. In fact, this effect was the reason for the diction that molecular surface mass spectrometry had to be performed in the so-called static mode, where it was ensured that the projectile fluence applied in the course of an entire analysis was small compared with that needed to remove a monolayer equivalent of the sample (the “static limit”). On the basis of static SIMS, molecular information about regions located below the immediate surface could therefore only be obtained by using relatively coarse microsectioning tools, for example cryosectioning or freeze fracture.

The above scenario is nearly always observed if atomic ion beams are used for sputter erosion and analysis. With ion fluence accumulating beyond the static limit, an exponential decay of molecule-specific mass spectral signals is found, which can be described by an apparent “disappearance cross section” of the order of 0.1…10 nm^2. This property indicates that molecular information is reduced to essentially zero throughout the removal of about one monolayer. On the other hand, it was discovered earlier [2] that this situation changes if *cluster* projectiles are used to bombard the surface. Not only are these projectiles found to greatly increase the yield of molecular ion species in the sputtered flux (thereby greatly enhancing their detection sensitivity, as reviewed elsewhere [3,4]), but also to largely suppress the fluence-dependent disappearance of the molecular signal, opening the door for molecular sputter depth profiling applications. This knowledge was not utilized in surface mass spectrometry for many years because of the complexity of the equipment needed to produce reliable cluster ion beams of sufficient intensity. Only recently, the advent of commercially available technology delivering intense, highly focusable cluster ion beams has dramatically changed this situation. Primary ion beams which are now routinely used for SIMS analysis feature various different cluster projectiles including C_n, Au_n, Bi_n, and Ar_n with values of n ranging from 2 to several thousand. For the specific case of organic samples, carbon clusters appear to be ideal projectiles, because of mass matching with the carbon atoms in the sample. Moreover, it was assumed that carbon atoms from the projectile would not induce unwanted chemical reactions in the surface material for these types of samples. As a consequence, great efforts have been devoted to the development of carbon cluster ion sources and to fundamental investigations of the interaction of such projectiles with organic solids. As a first step in this direction, Gillen et al. [5] used a cesium ion sputtering technique to generate a C_n^- cluster ion beam with n=2 … 10. As shown in the following section, they found that molecular depth profiling of an organic film worked with these projectiles, the results being better with larger values of n. Attempts to use metal clusters (Al_n) generated by the same technique, on the other hand, seemed to be much less successful, indicating the unique role of C_n projectiles for such a task [6]. On the basis of these findings, significant effort was devoted to developing a fullerene cluster ion source for use in surface mass spectrometry [7]. As of today, C_{60}^{q+} ion beams delivered by such a device seem to be the most versatile tools for sputter depth profile analysis of organic molecular samples. From a rapidly growing number of studies performed on various model systems [5,7–29], insights into the fundamental concepts and mechanisms governing the cluster–solid interaction process behind molecular sputter depth profiling are beginning to emerge. In parallel, applications of these ion beams to real-world samples are actively being pursued, with the ultimate objective of three-dimensional location of specific molecules by combining molecular depth profiling with laterally resolved microanalysis [18,30–35]. These experiments open the door to a wide range of possible applications in organic thin-film technology, biochemistry, and biology. As an example, it has recently been demonstrated that the technique enables the spatial location of specific biomolecules within single cells [33,35].

While this paper is restricted to the discussion of carbon cluster projectiles, it should be noted for completeness that other cluster ion beams (small metal [17], reactive ion [18,22,36,37], large rare gas [38], or giant glycerol [39] clusters) may, in principle, also be employed for molecular depth profiling. Although some of these have been shown to work rather well for

specific types of samples, carbon cluster ion beams seem to be the most versatile probes for molecular sputter depth profiling available to date.

Experimental findings

This section briefly reviews some of the findings on sputter depth profiling of organic material in combination with SIMS using carbon cluster ion beams. The experimental data reported below have been acquired in two ways. With the first method, a dynamic SIMS microscope was equipped with a cesium-sputtering ion source [5] delivering C_n^- cluster projectiles with n=1 … 10. With the second method, ToF-SIMS instrumentation [40,41] was employed in combination with a fullerene cluster ion gun [7] delivering C_{60}^{q+} ions of selectable charge state q=1 … 3 with kinetic energies up to several 10q keV. In some cases, mass spectral data acquisition was performed using the same focused fullerene ion beam as used for sputter erosion. Alternatively, the fullerene gun was solely used for erosion, while acquisition of SIMS data was performed using a liquid metal Au_n^+ or Bi_n^+ ion source.

Information about the chemical composition of the sample as a function of the vertical dimension along the surface normal (in the following text referred to as “depth”) is obtained by acquiring mass spectral data separated by sputtering cycles, where the surface is eroded by the ion beam. Conversion of the applied projectile ion fluence into eroded depth is usually accomplished by inspection of the eroded crater using stylus profilometry, atomic-force microscopy, or optical interferometry after completion of the depth profile analysis. Depending on the nature of the sample, the resulting depth scale calibration is generally non-linear, because different layers of the sample may exhibit different erosion rates [24]. This is particularly important for the analysis of organic films on inorganic substrates (for example Si, Ag, etc.), where the erosion rate may change by orders of magnitude upon transition through the interface.

Projectile size effects

The role of projectile nuclearity, i.e., the number of carbon atoms in a projectile cluster ion, was studied by Gillen et al. [5] who investigated a glutamate film on a silicon substrate using C_n^- primary ions. A reproduction of their data is shown in Fig. 1. The $(M-H)^-$ molecular secondary ion signal is plotted as a function of the erosion time using C_2^-, C_4^-, C_6^-, or C_8^- projectile ions. It is evident that the diatomic projectile still produces a fluence dependence which is typical for atomic ions, namely a simple exponential decay of the molecule specific signal to essentially zero. After conversion of the bombardment time into primary ion fluence, one can use the slope to determine an apparent disappearance cross section of the order of several nm^2. It is evident that this signal variation has nothing to do with the true abundance distribution of the analyte molecules in the sample. In contrast, the same profile recorded under C_6^- and C_8^- ion bombardment seems to represent the overlayer structure very well. In fact, both profiles exhibit all features of a typical molecular depth profile, namely an initial exponential decay into a steady state region, where the molecule-specific signal persists until the entire overlayer has been removed by ion erosion. At this point, the signal sharply drops, accompanied by a corresponding rise of substrate-specific secondary ion signals. The initial decay of the molecular ion signal can be interpreted in terms of a simple model describing the erosion and fragmentation dynamics (see “Discussion” section).

The profile recorded with C_4^- projectiles exhibits intermediate behavior. After the initial (fast) exponential decay, a steady state seems to be established for a short time; this is then followed by a second, slower exponential decay of the molecule specific signal. Profiles of this kind have been observed for other systems also, where the decay of the molecular ion signal in this “quasi-steady-state” region was attributed to a corresponding decay of the removal rate. Further examples of such a behavior will be shown below.

C_{60} depth profiling

Soon after the introduction of a fullerene ion source for use in surface mass spectrometry, Vickerman and coworkers [7,42] observed surprisingly low disappearance cross sections for molecular ion signals measured on some organic films, indicating that molecule-specific information may persist beyond the static limit under bombardment with C_{60} projectile ions. Following these observations, Sun et al. [43] demonstrated the possibility of not only *retaining* but even *enhancing* molecular ion signals of biomolecules by bombardment with C_{60} cluster ions to fluences far beyond the static limit. Their data are reproduced in Fig. 2, obtained for histamine molecules embedded in a frozen ice matrix. The molecular ion signal is initially very low, because the sample is covered by a cap of pure ice. Under irradiation with cluster projectiles, the cap is removed and the signal of histamine molecules is found to increase by two orders of magnitude. Switching the bombardment to atomic ions (Ga^+) leads to the well-known exponential signal decay, while switching back to C_{60}^+ quickly restores the molecular ion signal. This is a key observation, because it demonstrates that carbon cluster sputtering may even be able to remove the chemical damage created by previous bombardment using atomic ions, a notion which had previously been observed for SF_5^+ primary ions [8] also. With C_{60} projectiles, the same result was later confirmed for other molecular films as well [31].

Examples of molecular depth profiles measured on different organic overlayers on Si using C_{60}^+ projectile ions are shown in Fig. 3. Figure 3a and b refer to single films deposited either by spin-casting (a) or by thermal evaporation (b). In both cases, the molecular ion signal exhibits the typical ion fluence dependence depicted already in Fig. 1, namely an initial exponential decrease into a well-developed steady state, followed by a relatively sharp decay as the film–substrate interface is reached. It should be noted in passing that the same films analyzed with Au_3^+ cluster ions yield much more distorted profiles with at least an order of magnitude lower steady-state signal values than those observed in Fig. 3 [16,44]. Figure 3c shows a profile of an organic multilayer stack, which has been built from individual films deposited using the Langmuir–Blodgett technique. It is seen that the sequence of individual layers of about 50 nm thickness can be clearly resolved. Figure 3d depicts the result of a delta layer experiment [29] in which the signal response of thin layers of a polymer additive embedded into a matrix of a different material is followed as a function of projectile ion fluence. Experiments of this type are often used to characterize the depth resolution. It should be stressed again that molecular depth profiles like those displayed in Fig. 3 have long been impossible to acquire when atomic ion beams were mainly used for sputter erosion. Using cluster projectiles, on the other hand, the molecular ion signal variation clearly reveals the multilayered structure of the investigated sample, illustrating the fundamental difference between the surface erosion processes initiated by atomic and cluster ion beams.

Depth resolution

If data of the kind depicted in Fig. 3 are to be interpreted in terms of real composition depth profiles, the accumulated primary ion fluence must be converted into eroded depth. Particularly when profiling across interfaces between different layers, this conversion is not straightforward, because erosion rates may vary from one layer to the other. For organic material irradiated with C_{60} cluster projectiles, sputter yields are typically high, leading to the removal of about 100 nm^3 of sample volume per projectile impact, with differences between different samples typically being modest (factors of 2). This is different for a film–substrate interface, where the sputter yield may drop by orders of magnitude between the organic film and the inorganic substrate material. An accurate correction for the erosion rate variation is difficult. As a first-order approximation, one can use a linear interpolation scheme with weight factors calculated from the acquired mass spectral data [16,17,24,45], but this approach is still under debate because sputter yields of multicomponent systems may exhibit large

nonlinearities as a function of chemical composition [46]. The average erosion rates of different materials can be determined from the ion fluence needed to remove a layer of known thickness. Care must be taken, however, regarding the exact definition of the interface. In the profiles of Fig. 3, one can see that the interface location determined from the decrease of the film signal is not exactly equivalent to that determined from the rise of the substrate signal, indicating the presence of additional (oxide or hydroxide) interlayers between the organic film and the actual Si substrate [47].

Following depth scale calibration, the apparent depth resolution is generally evaluated from the measured 84%–16% interface width. In cases like the one displayed in Fig. 3c, where film thickness and interface width are comparable and, hence, no steady-state plateaus are reached, the “interface width” can be determined from the signal modulation contrast [21], whereas in the extreme case of a delta layer (Fig. 3d) it is simply evaluated from the width of the signal response function [29]. The apparent depth resolution observed in molecular depth profiles is typically rather large (of the order of 10 nm) compared with high-resolution inorganic depth profiling. A detailed discussion of different contributions influencing this quantity can be found elsewhere [48]. From the limited data set available to date, it seems that measured interface widths must at least partly reflect the build-up of surface micro-topography arising from the statistical nature of the sputtering process [49].

Effect of impact conditions

In addition to the choice of the projectile species, selectable conditions affecting the outcome of a molecular depth profile are the impact energy and angle of the eroding ion beam. For the cholesterol film depicted in Fig. 3b, the resulting effect is illustrated in Fig. 4. It is seen that the depth profile changes quite dramatically if the impact angle is changed from oblique to normal incidence (angles referenced to the surface normal). In the latter case, a gradual decrease of the molecular ion signal is observed after the initial exponential decay instead of a steady state throughout the removal of the film. In fact, the profile measured under these conditions resembles that displayed for C_4 projectiles in Fig. 1. As explained below and described in detail elsewhere [25,26,29,50], this behavior can be related to a steadily decreasing sputter yield while eroding through the organic film. Apparently, this yield-quenching effect is much less pronounced if the impact angle is changed to oblique incidence. At the same time, the initial signal drop is found to become less pronounced, indicating less beam-induced fragmentation under oblique incidence. For polymer samples, this notion is supported by XPS data obtained under C_{60} bombardment at different impact angles [51].

Interestingly, the largest sputter yield is found for medium impact angles near 45 degrees. Qualitatively, this finding can be rationalized as follows [52]. At normal incidence, the projectile penetrates the surface as a whole before breaking apart, thereby depositing its energy deeper into the sample. Upon transition to oblique incidence, the energy density deposited immediately below the surface increases, leading to more efficient sputtering. If the impact angle becomes too large, on the other hand, a sizeable fraction of the projectile atoms start to be reflected from the surface, thereby reducing the deposited energy density again.

The effect of impact energy is illustrated in Fig. 4c and d. In combination with the profile depicted in Fig. 3b, one can see that the major effect is related to the steady-state level of the molecular ion signal. Apparently, higher impact energy leads to a larger influence of beam-induced fragmentation, a finding which seems intuitively reasonable. A more quantitative discussion of this behavior is given below. The sputter yield under C_{60} impact is found to increase linearly with impact energy, an observation which has been found for many other organic materials also [53].

Temperature effects

An interesting observation relates to the effect of sample temperature on the outcome of a molecular depth profile. In fact, some of the data displayed in Fig. 3 were obtained with the sample stage cooled to liquid nitrogen temperature. If the same analysis is performed at different temperatures, one obtains data like those shown in Fig. 5. While the trehalose/peptide profile looks qualitatively similar at both temperatures, close inspection reveals a higher steady state signal at low temperature, indicating less fragmentation if the sample is cooled. The LB multilayer experiment performed at room temperature reveals a dramatic loss of both signal level and depth resolution with increasing eroded depth. At the same time, the erosion rate is found to decrease as a function of projectile ion fluence, indicating a reduction of the sputter yield. As can be seen in Fig. 5b, the yield-quenching effect is largely absent if the sample stage is cooled. Interestingly, the yield-quenching effect seems to return if the impact energy is raised while the sample is kept at low temperature [26].

The exact reason for these observations is currently unclear. One can speculate from these experiments, however, that both the sputter yield and the fragmentation dynamics must be affected by impact-induced surface chemistry. In particular, yield quenching under C_{60} ion impact has been observed for other systems also [25,54–58] and seems to be an ubiquitous effect accompanying carbon cluster bombardment of both organic and inorganic samples. Note, however, that a similar observation to that in Fig. 5a has also been made for polymer samples under bombardment with SF_5^+ ions [15]. In any case, the effect must be provoked by chemical reactions that are activated by radiation-enhanced mobility of species at or below the surface. For carbon cluster bombardment, a possible scenario one could imagine involves the incorporation of projectile atoms into the near surface region, which may then aggregate and nucleate to form amorphous carbon precipitates with extremely low sputter yield. For the specific case of polymer samples, co-bombardment with low-energy argon ions has been demonstrated to reduce the problem [59], but application of this technique to other organic films has proven less successful [60].

Discussion

Erosion dynamics

Using a simple phenomenological model [17,28,50], the general features of a molecular depth profile can be easily rationalized. Based on the ideas sketched originally by Williams and Gillen [61], the observed signal dynamics are governed by a competition between ion induced *fragmentation* and *removal* of material present at the bombarded surface. If the removal rate is slow, fragmentation dominates, leading to accumulation of beam-induced chemical damage which manifests as an exponential disappearance of the molecule specific secondary ion signal. Note that this situation is fulfilled for practically all atomic primary ions, because of the limited sputter yield of organic material that can be achieved with these projectiles. Under these conditions, molecular information can only be obtained in the static regime. The signal decay as a function of projectile ion fluence can be parametrized by a disappearance cross section of typically 1 … 10 nm^2. If, at the other extreme, sputter removal is fast compared with fragmentation, the debris produced by a projectile impact may be efficiently removed in the course of the same event, thereby exposing fresh undamaged molecules for analysis in later impact events. In this limit, the molecular ion signal would ideally persist at its static level until the organic overlayer has been completely removed. In intermediate cases where damage and removal rates are comparable, the molecular ion signal is expected to drop exponentially into a steady state level reflecting the respective ratio between damage and removal rates.

Using this model, one can relate the observed steady-state signal level to a “cleanup efficiency”, defined as the ratio between the average sample volume *removed* and *damaged* per projectile

impact, respectively. The former is described by the sputter yield volume (measured in nm^3/impact), while the latter can be parametrized as the product of a lateral damage cross section and the depth of the surface layer altered by the ion bombardment. As described in detail elsewhere [17,28,50], analysis of the entire signal evolution as a function of projectile ion fluence allows values for these properties to be determined separately. The calculation leads to sputter yield volumes, damage cross sections, and altered layer thicknesses of typically 100 nm^3, 10 nm^2, and 10 nm, respectively. Mostly because of the large sputter yields achieved with such projectiles, cluster bombardment is often connected with cleanup efficiencies ε of the order of unity, which translate into a steady-state molecular ion signal level $S_{SS}/S_0 = \varepsilon/(1 + \varepsilon)$ that is comparable with the original (static) value S_0. In contrast, atomic ion bombardment leads to significantly lower sputter yields (of the order of 1 nm^3/impact), whereas damage cross section and altered layer depth remain comparable with those prevailing under cluster irradiation. In fact, 15-keV Ga^+ bombardment of a sugar film has been demonstrated to create a damaged sub-surface layer as much as about 50 nm thick [30,31]. As a consequence, the cleanup efficiency achievable with atomic projectiles is extremely low, leading to an accumulation of the chemical damage with correspondingly low values of the steady-state molecular signal [62].

In principle, the cleanup efficiency can be directly determined from the signal drop between the original (static) molecular ion signal and its steady-state value. For the data presented in Figs. 1, 3, and 4, the resulting values are displayed in Table 1. A few trends can be observed. First, it is evident that the cleanup efficiency increases with increasing projectile nuclearity if all other conditions are kept constant. Second, the cleanup efficiency increases with decreasing projectile impact energy. C_8 clusters of about 3 keV seem to have values comparable with those of 40-keV C_{60} clusters, a notion which is understandable because both relate to about the same energy per constituent projectile atom. Note that under 40-degree impact of C_{60}^+ projectile ions with kinetic energies of 20 keV or below, the molecular ion of cholesterol exhibits a very small (Fig. 4c) or no [44] fluence-dependent degradation at all, indicating $\varepsilon \gg 1$. As a function of impact angle, the cleanup efficiency is found to be approximately constant between 0 and 45 degrees and to strongly increase under more oblique incidence. In addition, the apparent depth resolution is improved with increasing impact angle, a finding which is true for single films [25] and for multilayer samples [26]. As a consequence, one must conclude that low impact energy combined with oblique incidence should generally represent favorable conditions for successful molecular depth profiling.

The erosion dynamics model can also be utilized to rationalize the “unusual” behavior of depth profiles like that depicted in Fig. 1 (C_4 projectiles), Figure 4a, and Fig. 5b (RT profile). Since the steady-state reflects the cleanup efficiency, changes of the ratio between sputter yield volume and damage volume must directly translate into respective changes of the molecular ion signal. Because both the damage cross-section and the altered layer depth are not expected to vary significantly with accumulating ion fluence, the yield-quenching effect observed for certain organic materials under fullerene ion bombardment [29,55,57,63] therefore leads to a corresponding signal decrease which is observed in these profiles. If the decay rate is slow compared with the initial exponential decay, one can approximate the respective signal variation by the steady-state solution of the model equations and refer to this as a “quasi-steady-state” condition. Details of the respective formalism can be found elsewhere [50]. Since the sputter yield variation can, in principle, be measured independently, using the ion fluence needed to remove a known layer thickness, the resulting prediction can be compared with the measured signal variation, thus enabling quantitative testing of the model [25,26,29,50].

Ionization effects

Besides the ability to erode without damage accumulation, cluster ion beams offer the advantage of a significantly increased molecular ion signal. This effect is already visible in the data presented in Fig. 1, where C_8^- is found to enhance the static $(M-H)^-$ signal of glutamate by about two orders of magnitude compared with that measured under bombardment with atomic C^- ions of the same impact energy. For C_{60} projectiles, one finds even larger signal enhancements up to three orders of magnitude when compared to atomic projectiles such as Ga^+ or Au^+. In part, these enhancements are caused by the larger sputter yields under cluster bombardment. It is interesting to note, however, that the molecular ion yield enhancement is generally larger than that of the sputter yield (by a factor of 50 for trehalose upon switching from Au^+ to C_{60}^+ projectiles [17]). Moreover, molecule-specific secondary ions appear to be more strongly enhanced than smaller fragment ions, indicating a smaller degree of fragmentation during the desorption process under cluster bombardment.

Another interesting question is whether the apparent increase in secondary ion yield might in part be caused by an increased *ionization probability* of the desorbed molecules. In fact, it has been speculated that C_{60} bombardment might help the chemical ionization process by, for instance, liberating protons to form $(M+H)^+$ molecular ions [3,4,64]. In that respect, the initial signal transients observed at the beginning of the profiles shown in Fig. 3a and Fig. 4b, c have been tentatively attributed to fluence-dependent changes of the ionization probability of sputtered intact molecules [16].

In order to clarify this question, it is necessary to simultaneously detect the desorbed *neutral* and *ionized* molecules under otherwise identical experimental conditions. This experiment, in turn, requires post-ionization of sputtered molecular species, a task which is not straightforward because of the risk of fragmentation in the course of the ionization process. Using strong-field photoionization in an intense, short-pulse infrared laser beam, Willingham and coworkers [65] have recently acquired a simultaneous depth profile of neutral parent molecules (M^0) and molecular secondary ions $(M+H)^+$ from a 170-nm guanine film on a silver substrate. Their data are reproduced in Fig. 6. It is seen that the neutral molecule signal follows the purely exponential decay into a steady state value predicted by the erosion dynamics model. In contrast, the secondary ion signal exhibits an initial surface transient which must be caused by variations of the ionization probability. In fact, the evolution of this quantity can be easily determined by plotting the $(M+H)^+/(M^0)$ signal ratio as depicted in Fig. 6c.

From Fig. 6, it is seen that the chemical ionization probability of sputtered guanine molecules exhibits a fast initial rise during removal of the first few nanometers. Apparently, the accumulation of C_{60} projectile ion fluence leads to a surface modification which helps forming $(M+H)^+$ secondary ions in the course of the desorption event. The effect, however, is not very large (about a factor of two). In addition, the ionization probability is found to drop by about two orders of magnitude after crossing the film–substrate interface. It is evident from the figure, however, that this change does not significantly influence the location or width of the interface. This finding is important, because matrix-dependent changes in ionization probability may in principle dramatically influence the interface behavior of a secondary ion signal. Nevertheless, these effects need to be kept in mind when interpreting molecular SIMS depth profiles.

Conclusions

The advent of commercially available cluster ion beam technology has marked a breakthrough in surface and thin-film analysis by making sputter depth profiling of molecular systems feasible, a task which was long deemed impossible because of the accumulation of chemical damage. The general picture behind this observation is that a cluster projectile deposits its energy closer to the surface, thereby generating more “action” immediately at and less damage

deeper below the surface. The data available so far indicate that carbon cluster ions might be among the most versatile projectiles for analysis of organic material, if the yield-quenching effect can be understood and controlled. Using fullerene cluster ion beams, sputter depth profiling in combination with molecular surface mass spectrometry has matured into a technique which may be routinely used in the future. Using model systems as a simple and reproducible platform, fundamental issues regarding the desorption process, sputter erosion, fragmentation, and ionization dynamics under cluster impact, and the depth resolution achievable with this technique, are currently being addressed. In particular, the role of different conditions regarding both the ion beam and the investigated sample is studied in order to find optimized conditions for successful molecular depth profiling. From these experiments, a fundamental insight into the concepts behind the cluster–surface interaction is beginning to emerge.

The data presented here open the door for many applications in thin film technology, biochemistry, and biology. Because of the polyatomic nature of the projectiles, high-energy primary ion beams can be used which are focusable to sub-micron spot size. As a consequence, the three-dimensional chemical analysis of organic thin film structures has become feasible, a task which will be invaluable for the design processes in fields such as molecular electronics. Moreover, one can think of locating specific molecules within biological objects, for example single cells. These concepts are currently being explored with promising results.

Acknowledgments

Financial support from the National Institute of Health under grant # EB002016-16, the National Science Foundation under grant # CHE-0555314, and the Department of Energy grant # DE-FG02-06ER15803 are acknowledged

References

1. Benninghoven, A.; Rüdenauer, FG.; Werner, HW. Secondary Ion Mass Spectrometry: basic concepts, instrumental aspects and trends. Wiley; New York: 1987.
2. Cornett DS, Lee TD, Mahoney JF. Rapid Commun Mass Spectrom 1994;8:996–1000. [PubMed: 7696706]
3. Winograd N. Anal Chem 2005;77:142A–149A.
4. Wucher A. Appl Surf Sci 2006;252:6482–6489.
5. Gillen G, Lance K, Freibaum B, Lareau RT, Bennett J, Chmara F. J Vac Sci Technol 2001;19:568–575.
6. Gillen, G. personal communication.
7. Weibel DE, Wong S, Lockyer N, Blenkinsopp P, Hill R, Vickerman JC. Anal Chem 2003;75:1754–1764. [PubMed: 12705613]
8. Gillen G, Roberson S. Rapid Commun Mass Spectrom 1998;12:1303–1312. [PubMed: 9773521]
9. Fuoco ER, Gillen G, Wijesundara MBJ, Muthu BJ, Wallace WE, Hanley L. J Phys Chem B 2001;105:3950–3956.
10. Gillen G, Fahey A. Appl Surf Sci 2003;203/204:209–213.
11. Wucher A, Sun S, Szakal C, Winograd N. Appl Surf Sci 2004;231/232:68–71.
12. Mahoney C, Roberson S, Gillen G. Anal Chem 2004;76:3199–3207. [PubMed: 15167802]
13. Wagner MS, Gillen G. Appl Surf Sci 2004;231/232:169–173.
14. Wagner MS. Anal Chem 2005;77:911–922. [PubMed: 15679361]
15. Mahoney C, Gillen G, Fahey A, Zu Ch, Batteas J. Appl Surf Sci 2005;252:6502–6505.
16. Cheng J, Winograd N. Anal Chem 2005;77:3651–3659. [PubMed: 15924401]
17. Cheng J, Wucher A, Winograd N. J Phys Chem B 2006;110:8329–8336. [PubMed: 16623517]
18. Gillen G, Fahey A, Wagner M, Mahoney C. Appl Surf Sci 2006;252:6537–6541.
19. Fletcher JS, Conlan XA, Lockyer N, Vickerman JC. Appl Surf Sci 2006;252:6513–6516.

20. Jones EA, Fletcher JS, Thompson CE, Jackson DA, Lockyer NP, Vickerman JC. Appl Surf Sci 2006;252:6844–6854.
21. Zheng L, Wucher A, Winograd N. J Am Soc Mass Spectrom 2007;19:96–102. [PubMed: 18293488]
22. Mahoney C, Fahey A, Gillen G. Anal Chem 2007;79:828–836.
23. Jones EA, Lockyer NP, Vickerman JC. Anal Chem 2008;80:2125–2132. [PubMed: 18278949]
24. Wucher A, Cheng J, Winograd N. Appl Surf Sci 2008;255:959–961.
25. Kozole J, Wucher A, Winograd N. Anal Chem 2008;80:5293–5301. [PubMed: 18549239]
26. Zheng L, Wucher A, Winograd N. Anal Chem 2008;80:7363–7371. [PubMed: 18778034]
27. Zheng L, Wucher A, Winograd N. Appl Surf Sci 2008;255:816–818. [PubMed: 19551160]
28. Wucher A, Cheng J, Winograd N. J Phys Chem C 2008;112:16550–16555.
29. Shard AG, Green FM, Brewer PJ, Seah MP, Gilmore IS. J Phys Chem B 2008;112:2596–2605. [PubMed: 18254619]
30. Wucher A, Cheng J, Zheng L, Willingham D, Winograd N. Appl Surf Sci 2008;255:984–986.
31. Wucher A, Cheng J, Winograd N. Anal Chem 2007;79:5529–5539. [PubMed: 17583913]
32. Vaidyanathan S, Fietcher JS, Goodacre R, Lockyer NP, Micklefield J, Vickerman JC. Anal Chem 2008;80:1942–1951. [PubMed: 18290669]
33. Fletcher JS, Rabbani S, Henderson A, Blenkinsopp P, Thompson SP, Lockyer NP, Vickerman JC. Anal Chem 2008;80:9058–9064. [PubMed: 19551933]
34. Fletcher JS, Lockyer NP, Vaidyanathan S, Vickerman JC. Anal Chem 2007;79:2199–2206. [PubMed: 17302385]
35. Malmberg P, Kriegeskotte C, Arlinghaus HF, Hagenhoff B, Holmgren J, Nilsson M, Nygren H. Appl Surf Sci 2008;255:926–928.
36. Mahoney C, Roberson S, Gillen G. Appl Surf Sci 2004;231/232:174–178.
37. Mahoney C, Fahey A, Gillen G, Xu C, Batteas J. Anal Chem 2007;79:837–845.
38. Ichiki K, Ninomiya S, Nakata Y, Honda Y, Seki T, Aoki T, Matsuo J. Appl Surf Sci 2008;255:1148–1150.
39. McMahon JM, Dookeran NN, Todd PJ. J Am Soc Mass Spectrom 1995;6:1047–1058.
40. Braun RM, Blenkinsopp P, Mullock SJ, Corlett C, Willey KF, Vickerman JC, Winograd N. Rapid Commun Mass Spectrom 1998;12:1246–1252. [PubMed: 9772767]
41. Niehuis E, Heller T, Feld H, Benninghoven A. J Vac Sci Technol A 1987;5:1243–1246.
42. Weibel DE, Lockyer N, Vickerman JC. Appl Surf Sci 2004;231/232:146–152.
43. Wucher A, Sun S, Szakal C, Winograd N. Anal Chem 2004;76:7234–7242. [PubMed: 15595864]
44. Jones EA, Lockyer NP, Vickerman JC. Int J Mass Spectrom 2007;260:146–157.
45. Wagner MS. Anal Chem 2004;76:1264–1272. [PubMed: 14987080]
46. Betz, G.; Wehner, GK. Sputtering of Multicomponent Materials. In: Behrisch, R., editor. Sputtering by Particle Bombardment. Vol. 2. Springer; Heidelberg: 1983.
47. Green FM, Shard AG, Gilmore IS, Seah MP. Anal Chem 2009;81:75–79. [PubMed: 19117445]
48. Wucher A, Cheng J, Zheng L, Winograd N. Anal Bioanal Chem 2009;393:1835–1842. [PubMed: 19153718]
49. Krantzman KD, Wucher A. J Phys Chem. 2009 submitted.
50. Wucher A. Surf Interface Anal 2008;40:1545–1551.
51. Miyayama T, Sanada N, Iida Si, Hammond JS, Suzuki M. Appl Surf Sci 2008;255:951–953.
52. Russo MF, Garrison BJ. Anal Chem 2006;78:7206–7210. [PubMed: 17037922]
53. Delcorte A. Appl Surf Sci 2008;255:954–958.
54. Gillen G, Batteas J, Michaels CA, Chi P, Small J, Windsor E, Fahey A, Verkouteren J, Kim KJ. Appl Surf Sci 2006;252:6521–6525.
55. Shard AG, Brewer PJ, Green FM, Gilmore IS. Surf Interface Anal 2007;39:294–298.
56. Shard AG, Green FM, Gilmore IS. Appl Surf Sci. In Press, Corrected Proof.
57. Fisher GL, Dickinson M, Bryan SR, Moulder J. Appl Surf Sci 2008;255:819–823.
58. Kozole J, Willingham D, Winograd N. Appl Surf Sci 2008;255:1068–1070. [PubMed: 19554201]

59. Yu B-Y, Chen Y-Y, Wang W-B, Hsu M-F, Tsai S-P, Lin W-C, Lin Y-C, Jou J-H, Chu C-W, Shyrue J-J. Anal Chem 2008;80:3412–3415. [PubMed: 18355087]
60. Bryan, S. Unpublished data shown at the AVS meeting; Boston. 2008.
61. Williams, P.; Gillen, G. Ion formation from organic solids. In: Benninghoven, A., editor. IFOS III. Springer; Berlin: 1988. p. 15-21.
62. Gillen G, Simons DS, Williams P. Anal Chem 1990;62:2122–2130. [PubMed: 2256549]
63. Moellers R, Tuccitto N, Torrisi V, Niehuis E, Licciardello A. Appl Surf Sci 2005;252:6509–6512.
64. Conlan XA, Lockyer NP, Vickerman JC. Rapid Commun Mass Spectrom 2006;20:1327–1334. [PubMed: 16555365]
65. Willingham D, Wucher A, Winograd N. J Chem Phys. 2009 submitted.
66. Gillen, G. personal communication.
67. Kozole J, et al. unpublished.
68. Gillen, G. personal communication.
69. Kozole J, et al. unpublished.

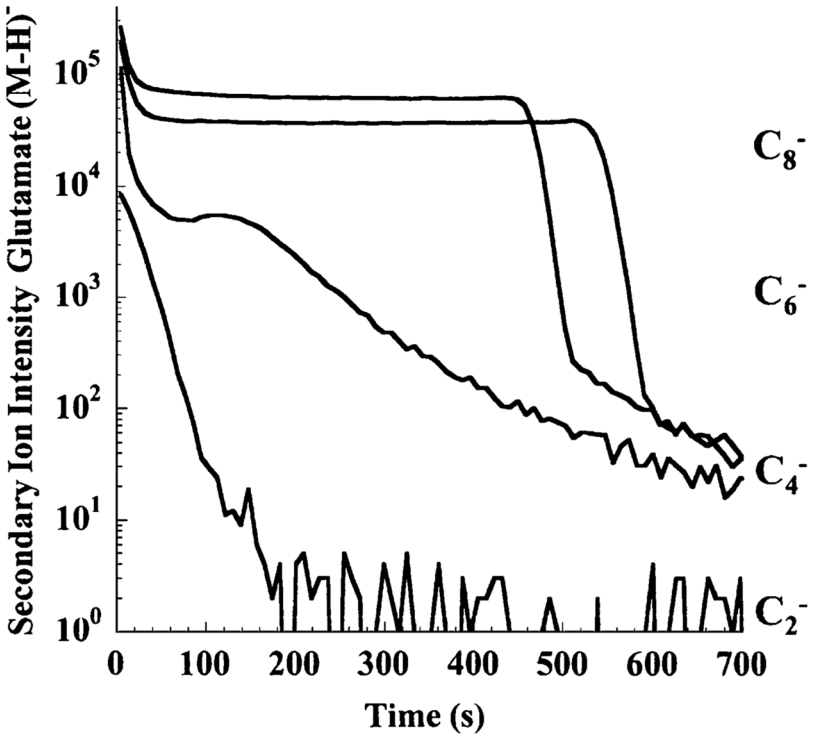

Fig. 1.

Molecular ion signal $(M-H)^-$ at *m*/*z* 146 representing a glutamate film on silicon as a function of sputtering time using 3-keV C_n^- projectile ions (reproduced with permission from Refs. [5,68])

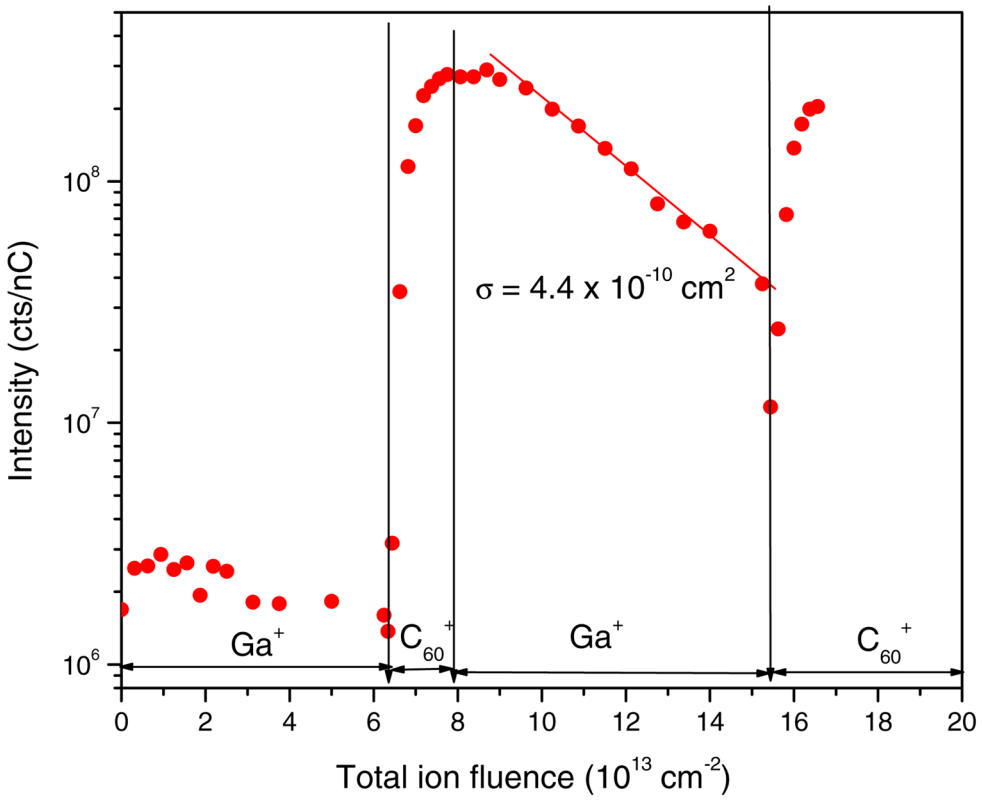

Fig. 2.

Molecular ion signal at *m*/*z* 111 of histamine embedded in a frozen ice matrix vs. accumulated primary ion fluence. The bombardment was switched between 20-keV C_{60}^+ and 15-keV Ga^+ ions at the indicated points (reproduced with permission from Ref. [43])

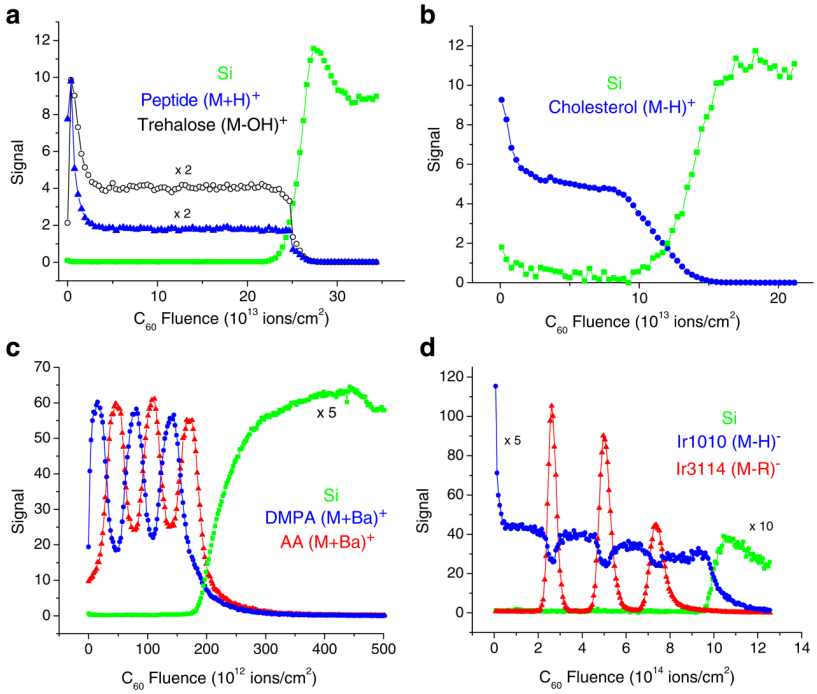

Fig. 3.

Molecular depth profile of (**a**) a 300-nm trehalose film doped with GGYR peptide, (**b**) a 300-nm cholesterol film, (**c**) a stack of six alternating LB multilayer films of barium arachidate (*AA*) and barium dimyristoyl phosphatidate (*DMPA*) approximately 50 nm wide, and (**d**) a sequence of Irganox3114 delta layers embedded in an Irganox1010 matrix (all films deposited on silicon) measured using C_{60}^+ projectile ions for sputter erosion and data acquisition (reproduced with permission from Refs. [16,25,26,29])

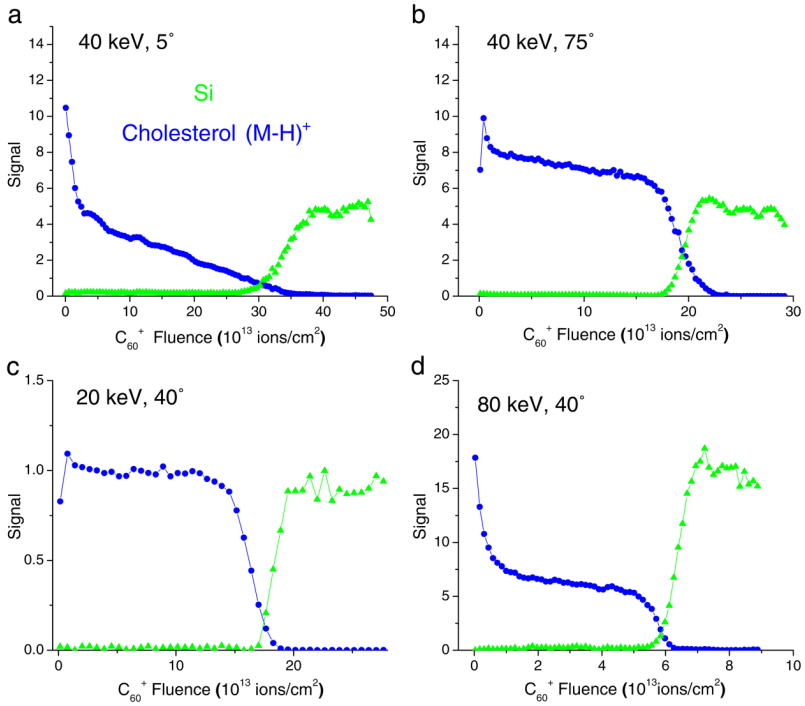

Fig. 4.

Molecular depth profiles of a 300-nm cholesterol film on Si using C_{60}^+ primary ions of different kinetic energies and impact angles (data reproduced from Refs. [25], [69])

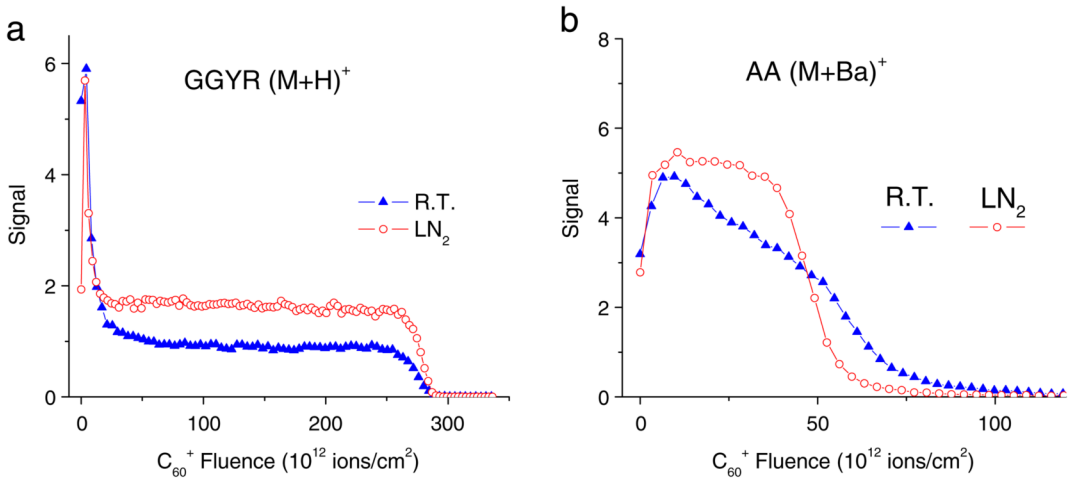

Fig. 5.

Molecular depth profiles of (**a**) a 300-nm trehalose film doped with peptide (GGYR) and (**b**) a 100-nm LB multilayer of barium arachidate (*AA*) on silicon measured with the sample at room temperature (*R.T.*) or cooled to liquid nitrogen temperature (LN_2). The profiles were acquired under otherwise identical experimental conditions using a 40-keV C_{60}^+ primary ion beam impinging under 40° with respect to the surface normal (data reproduced with permission from Refs. [16,26])

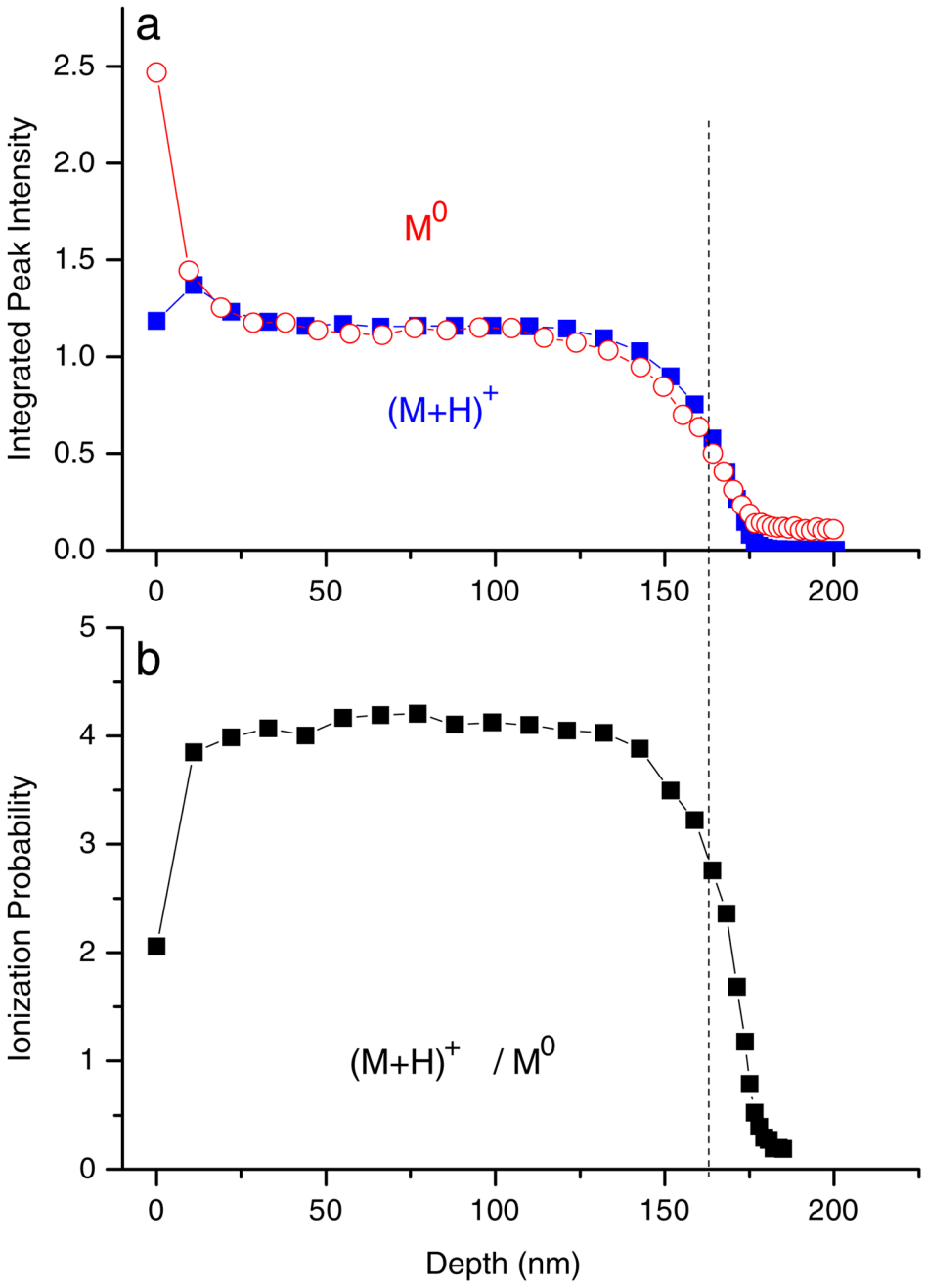

Fig. 6.

(**a**) Depth profile of neutral parent molecules (M^0) and molecular secondary ions $(M + H)^+$ sputtered from a 170-nm guanine film on silver under bombardment with 40-keV C_{60}^+ ions. (**b**) Ratio between secondary ion and neutral signal representing the ionization probability of the desorbed parent molecules (reproduced with permission from Ref. [65])

Table 1

Cleanup efficiency ε determined for different projectiles and molecular secondary ions. The values were calculated using data taken from the cited references

	Glutamate		Trehalose/peptide			Cholesterol	
[5,66]	$(M-H)^-$	[16,17,28]	$(M\text{-}OH)^+$	$(M+H)^+$	[25,67]	$(M\text{-}OH)^+$	$(M+H)^+$
3 keV C_2^-	$<3\times10^{-3}$	20 keV C_{60}^+	1.2	0.5	20 keV C_{60}^+, 40°	2.2	4.0
3 keV C_4^-	5×10^{-2}	40 keV C_{60}^+	0.5…1.3	0.2[a]	40 keV C_{60}^+, 40°	0.2	1.5
3 keV C_6^-	0.2	80 keV C_{60}^{2+}	0.7	–	80 keV C_{60}^{2+}, 40°	0.15	0.7
3 keV C_8^-	0.4	120 keV C_{60}^{3+}	0.4	–	40 keV C_{60}^+, 5°	0.3	0.9
					40 keV C_{60}^+, 73°	0.8	2.2

[a] For GGYR, values vary between 0.02 and 0.6 depending on peptide